

PHYSICAL METHODS
OF INVESTIGATION

Effect of the Synthesis Conditions on the Crystal, Local,
and Electronic Structure of $\text{Ce}_{1-x}^{3+}\text{Ce}_x^{4+}\text{AlO}_{3+x/2}$

V. V. Popov^a, A. P. Menushenkov^a, Ya. V. Zubavichus^b, A. S. Sharapov^a, V. A. Kabanova^a,
A. A. Yastrebtev^a, L. A. Arzhatkina^c, N. A. Tsarenko^c, A. M. Strel'nikova^c, and V. V. Kurilkin^d

^aNational Research Nuclear University MEPhI (Moscow Engineering Physics Institute),
Kashirskoe sh. 31, Moscow, 115409 Russia

^bNational Research Center Kurchatov Institute, pl. Akademika Kurchatova 1, Moscow, 123182 Russia

^cJSC All-Russian Research Institute of Chemical Technology, Kashirskoe sh. 33, Moscow, 115409 Russia

^dPeoples' Friendship University of Russia, ul. Miklukho-Maklaya 6, Moscow, 117198 Russia

e-mail: victorvpopov@mail.ru

Received July 2, 2015

Abstract—Cerium monoaluminate $\text{Ce}_{1-x}^{3+}\text{Ce}_x^{4+}\text{AlO}_{3+x/2}$ powders with low contents of Ce^{4+} cations ($x \sim 0.052$) were synthesized. A set of modern local structure sensitive methods of analysis, including X-ray absorption spectroscopy and Raman spectroscopy, were used to study the crystal, local, and electronic structures of the synthesized compounds. The degree of reduction and the thermal stability to oxidation of reduced powders depend not only on the reduction conditions but also on the conditions of heat pretreatment of the initial samples. It was concluded that the reaction $4\text{CeAlO}_3 + \text{O}_2 \leftrightarrow 4\text{CeO}_2 + 2\text{Al}_2\text{O}_3$ is reversible.

DOI: 10.1134/S0036023616020170

Cerium oxygen compounds are of considerable interest from the standpoint of inorganic synthesis and solid state chemistry owing to the ability of cerium cations to change the oxidation state depending on the preparation conditions. Therefore, the synthesis and study of the structure of compounds of this class have been attracting close researchers' attention [1–8]. In recent years, investigation of the structure of cerium compounds gained an additional impetus from the progress of modern methods for local structure investigation [7, 8]. It is noteworthy that cerium oxide-based materials are of considerable practical value for the production of catalysts [9], solid oxide fuel cells [10], polishing compositions [11], and for other purposes [4, 12].

Cerium monoaluminate CeAlO_3 , which has some specific structure details and physicochemical properties, is a cerium oxide compound that belongs to the class of lanthanide aluminates. Indeed, among complex cerium oxides containing Ce^{3+} cations, CeAlO_3 (as well as cerium hexaaluminate $\text{CeAl}_{11}\text{O}_{18}$) has enhanced thermal stability against oxidation, being decomposed during heat treatment in air at temperatures above 1000°C as a result of $\text{Ce}^{3+} \rightarrow \text{Ce}^{4+}$ oxidation to give CeO_2 and Al_2O_3 owing to the absence of interaction between components in the $\text{CeO}_2\text{--Al}_2\text{O}_3$ system [2]. At room temperature, CeAlO_3 has a distorted perovskite structure [1, 2]. However, there is

still no consensus in the literature concerning the type of symmetry of cerium monoaluminate crystals; there are data about tetragonal [13], orthorhombic [14], and other types of symmetry of CeAlO_3 observed both at room temperature and at elevated temperature [15]. It is noteworthy that CeAlO_3 is a promising material for the manufacture of microwave dielectric ceramics [13], various types of catalysts [16, 17] (including those having photocatalytic activity [18]), anodes for solid oxide fuel cells [10], etc.

The purpose of this work was to synthesize cerium monoaluminate CeAlO_3 and study its crystal, local, and electronic structures using a unique set of local structure sensitive X-ray diffraction and X-ray absorption methods, providing information about cationic ordering of the crystal lattice, and Raman spectroscopy, which gives information about anionic ordering of the complex oxide structures.

EXPERIMENTAL

The powders of CeAlO_3 were synthesized by reverse coprecipitation [19] of an aqueous solution of a $\text{Ce}(\text{NO}_3)_3 \cdot 6\text{H}_2\text{O}$ (99.99%) and $\text{Al}(\text{NO}_3)_3 \cdot 9\text{H}_2\text{O}$ (reagent grade) mixture (0.266 mol/L total salt concentration; atomic ratio $\text{Ce} : \text{Al} = 1 : 1$, pH 3.14) with aqueous ammonia (3.5 mol/L). The suspension thus formed (pH 9.80) was filtered, the resulting precipitate

Table 1. Synthesis conditions, designations, and composition of the synthesized powders

No.	Synthesis conditions	Designation	Color	TGA results		
				temperature range of mass change, °C	change in the sample mass, %	Composition
1	Fresh mixed hydroxide precipitate	CeAl_S	Violet			
2	Dried mixed hydroxide powder (precursor)	CeAl_P	Light yellow	30–1000	–23.40	$\text{Ce}_{0.036}^{3+}\text{Ce}_{0.0964}^{4+}\text{O}_{1.982} \cdot 1/2 \text{Al}_2\text{O}_3 \cdot 3.78\text{H}_2\text{O}$
3	Sample obtained by annealing the precursor at 1100°C/3 h in air	CeAl_1100A	Light yellow	100–740	–0.23	$\text{CeO}_2 \cdot 1/2\text{Al}_2\text{O}_3 \cdot 0.04\text{H}_2\text{O}$
4	Sample (2) reduced in a hydrogen flow at 1000°C/4 h	CeAl_P/1000H	Light gray	772–1070	+2.94	$\text{Ce}_{0.796}^{3+}\text{Ce}_{0.204}^{4+}\text{AlO}_{3.102}$
5	Sample (3) reduced in a hydrogen flow at 1000°C/4 h	CeAl_1100A/1000H	Light gray	865–1113	+3.52	$\text{Ce}_{0.948}^{3+}\text{Ce}_{0.052}^{4+}\text{AlO}_{3.026}$
6	Sample (3) heat treated in vacuum at 1400°C/3 h	CeAl_1100A/1400V	Light brown	930–1233	+3.52	$\text{Ce}_{0.948}^{3+}\text{Ce}_{0.052}^{4+}\text{AlO}_{3.026}$
7	Sample (6) heat treated in air at 1400°C/4 h	CeAl_1100A/1400V/1400A	Light yellow			$\text{CeO}_2 + \text{Al}_2\text{O}_3$

of mixed cerium aluminum hydroxide (precursor) was washed with distilled water and dried at 90°C for 8 h. The cation content in the filtrate was determined by inductively coupled plasma atomic emission spectroscopy (ICP-AES) using a Vista-PRO spectrometer (Varian, USA).

The dried powder (xerogel) was divided into two portions. One portion of the precursor xerogel was reduced in a hydrogen flow at 1000°C for 4 h, while the second one was subjected to isothermal annealing in air at 1100°C for 3 h. The resulting oxide powder was then reduced in two ways: in a hydrogen flow for 4 h at 1000°C and by isothermal annealing in vacuo (residual pressure of 1.33×10^{-3} Pa) for 3 h at 1400°C. The designations and the color of the samples are summarized in Table 1.

The thermogravimetric analysis (TGA) of the powders (precursor and reduced samples) was carried out using an SDT Q 600 thermal analyzer (TA Instruments) by heating at a 10 °C/min rate in a 30–1400°C temperature range in an air flow. The composition and the degree of reduction of the synthesized powders were determined by the thermogravimetric (TG) method from the change in the sample mass during heating to 1400°C and subsequent keeping at a constant temperature for 4 h in an air flow.

The crystal structure and phase composition of the resulting powders were studied by powder X-ray diffraction at the “Structural Materials Science” station of the Kurchatov synchrotron radiation source. The measurements were carried out in the transmission geometry at $\lambda = 0.68886$ Å and 150 mm sample–detector distance using an Imaging Plate Fuji Film BAS-5000 2D detector. The 2D patterns were integrated to the standard $I(2\theta)$ form using the Fit2D software [20]; the Rietveld full-profile analysis of X-ray diffraction patterns was carried out using the Jana2006 software [21].

The Ce L_3 -edge X-ray absorption near-edge spectra of the powders were recorded at the “Structural Materials Science” station of the Kurchatov synchrotron radiation source using a Si(111) monochromator and at the i811 station of the MAX-lab (Lund, Sweden). All measurements were carried out in the transmission mode using ionization chambers at room temperature. The XANES spectra were simulated using the XANDA software [22].

Raman spectra were measured at the shared use center of the Analytical Test Center of the JSC All-Russia Research Institute of Chemical Technology on a Nicolet iS50 spectrometer (Thermo Fisher Scientific Inc.) equipped with an additional Thermo Scientific iS50 Raman block, suitable for recording and Fourier transformation of the Raman spectra. The Raman spectra were measured under laser excitation ($\lambda = 1064$ nm) in the 100–3700 cm^{-1} range. The spectral

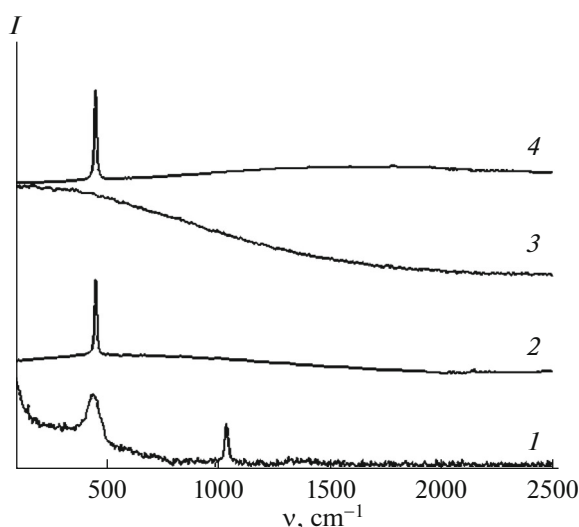


Fig. 1. Raman spectra of samples: (1) CeAl_P; (2) CeAl_1100A; (3) CeAl_1100A/1400V; (4) CeAl_1100A/1400V/1400A.

resolution was 4 cm^{-1} . The laser focusing point was chosen by means of a built-in optical microscope; the focused beam diameter on the sample was 50 μm .

RESULTS AND DISCUSSION

Initially, coprecipitation forms a brown-violet suspension, which indirectly attests to the presence of Ce^{3+} cation in the mixed cerium aluminum hydroxide precipitate. However, the dried precipitate was pale yellow-colored (Table 1), apparently, as a result of oxidation of cerium cations during drying of the precursor, the color being caused by the $\text{Ce}^{4+} \rightarrow \text{O}^{2-}$ charge transfer [15]. ICP AES analysis of the filtrate showed the absence of cerium ($<10^{-4}$ mg/L) or aluminum ($<5 \times 10^{-3}$ mg/L) cations in the liquid phase, which attested to complete precipitation of cations and provided the conclusion that the elemental composition (Ce : Al atomic ratio) of the synthesized solid oxide products corresponds to the amounts of initial salts taken for the reaction.

The results of X-ray diffraction attest to X-ray amorphous precursor structure. The Raman spectrum of the dried precursor powder shows two clear-cut peaks at 452 and 1049 cm^{-1} (Fig. 1, spectrum 1). The peak at 452 cm^{-1} is due to Ce–O vibrations in the CeO_2 fluorite structure [23]. The observed shift of the peak position relative to the CeO_2 reference (465 cm^{-1}) and large full width at half maximum ($FWHM = 62$ cm^{-1}) are likely to be due to the nano-sized state of the sample [24]. The peak at 1049 cm^{-1} is indicative of the presence of OH groups in the sample [25]. The cerium L_3 -edge XANES spectrum is split into two peaks,

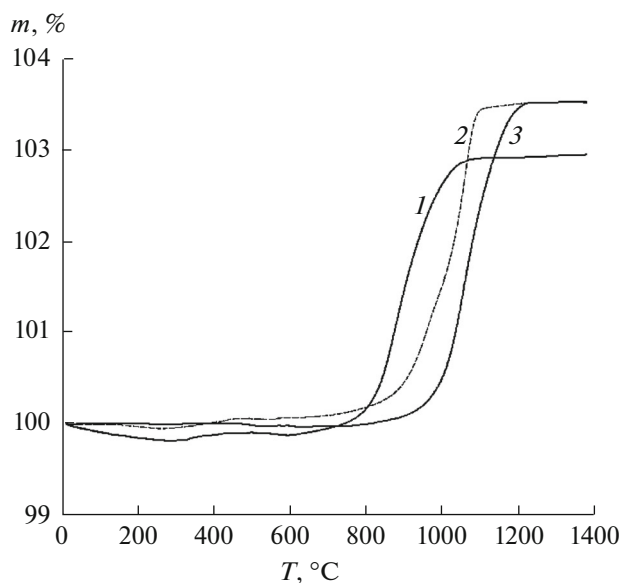


Fig. 2. Mass variation curves of reduced $\text{Ce}_{1-x}\text{Ce}_x\text{AlO}_{3+x/2}$ samples on heating in air: (1) CeAl_P/1000H; (2) CeAl_1100A/1000H; (3) CeAl_1100A/1400V.

which attests to the presence of Ce^{4+} cations in the dried sample. Hence, the dried precursor powder was, most likely, mixed cerium(IV) aluminum hydroxide.

A TGA study demonstrated that the decrease in the precursor weight upon dehydration occurs in several stages. The first stage corresponding to the removal of non-structural water present as adsorbed water molecules (–65% of the total mass loss) occurs in the temperature range of 30–235°C. The second stage corresponding to removal of a structure component as OH groups (–29%) occurs in the 235–482°C range. The residual water (–6%) is removed in the 482–1000°C temperature range. Further temperature rise to 1400°C resulted in a minor increase in the powder mass (+0.6% of the total mass change), probably, as a result of oxidation of the remaining Ce^{3+} cations to Ce^{4+} . From the TGA results, the proportion of Ce^{3+} in the precursor was calculated to be 0.036, while the composition of the dried precursor powder was found to be described as $\text{Ce}_{0.036}^{3+}\text{Ce}_{0.964}^{4+}\text{O}_{1.982} \cdot 1/2\text{Al}_2\text{O}_3 \cdot 3.78\text{H}_2\text{O}$.

The oxidation onset temperature of the reduced powders depends on the prehistory, i.e., on the conditions of heat pretreatment of the initial powders (Fig. 2). The sample prepared by the precursor reduction in a hydrogen flow at 1000°C/4 h had the lowest oxidation onset temperature (772°C), whereas the powder obtained by evacuation at 1400°C/3 h of the sample preannealed at 1100°C/3 h in air started to be oxidized

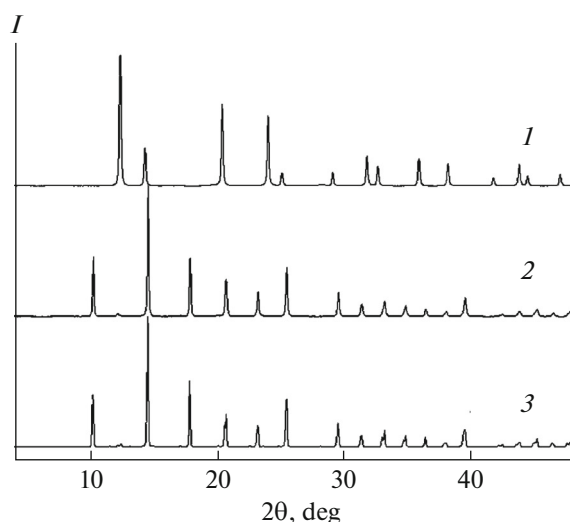


Fig. 3. General view of X-ray diffraction patterns of various types of synthesized samples: (1) CeAl_1100A; (2) CeAl_1100A/1000H; (3) CeAl_1100A/1400V.

at 930°C (Table 1). Quantitative treatment of the TGA data demonstrated that the composition of the reduced samples described by the general formula $\text{Ce}_{1-x}\text{Ce}_x\text{AlO}_{3+x/2}$ also depends not only on the reduction conditions but also on the conditions of heat pretreatment of the powders (Table 1). As can be seen from Table 1, the highest content of Ce^{4+} cations (i.e., the lowest degree of reduction) is inherent in the powder obtained by the reduction of the precursor.

The heat treatment in air affords pale yellow powders (irrespective of the temperature and duration). The powder X-ray diffraction study of the sample synthesized by isothermal annealing of the precursor at 1100°C/3 h (Fig. 3, pattern 1) demonstrated that this powder has a fluorite structure corresponding to CeO_2 (JCPDS No. 34-0394; cubic symmetry; space group $Fm\bar{3}m$ (225)) with the lattice parameter $a = 5.422 \text{ \AA}$ and coherent scattering length (CSL) of 37 nm. Detailed analysis demonstrated the presence of a minor impurity (~1%) of $\gamma\text{-Al}_2\text{O}_3$ (JCPDS No. 29-0063; cubic symmetry; space group $Fd\bar{3}m$ (227)) (Fig. 4a). These results are in good agreement with published data [2], which state that heating of the mixed Ce–Al hydroxide in oxidizing atmosphere at temperatures above 1000°C affords CeO_2 and Al_2O_3 . However, in [10], the Al_2O_3 phase was detected only after treatment of the CeAlO_3 powder at 1300°C in air. This does not contradict our results, because the observed Al_2O_3 reflection intensity for the sample (1100°C/3 h) is very low (Fig. 4a).

The reduced samples were colored in various shades of gray and brown, which attests to partial or

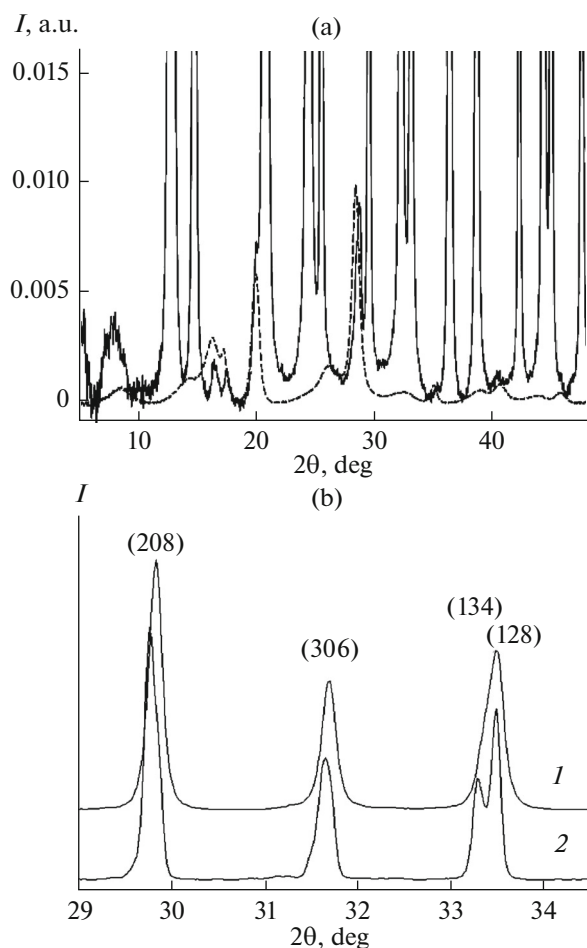


Fig. 4. (a) Detailed X-ray diffraction pattern of the CeAl_1100A sample (continuous line) and the γ -Al₂O₃ reference (dashed line). (b) Detailed X-ray diffraction patterns of reduced samples: (1) CeAl_1100A/1000H; (2) CeAl_1100A/1400V. The reflection indices of the corresponding planes are given in parentheses.

almost complete Ce⁴⁺ to Ce³⁺ reduction (Table 1). It was found by X-ray diffraction that the reduced samples mainly consist of cerium monoaluminate CeAlO₃ with a minor CeO₂ impurity (Fig. 3, patterns 2 and 3). The synthesized CeAlO₃ samples have a rhombohedral structure (JCPDS No. 21-0175; trigonal symmetry; space group $R\bar{3}m$ (166)). This is clearly seen while considering X-ray diffraction patterns in detail, especially for the sample obtained in vacuum (Fig. 4b). The CSLs are 40 nm for the sample reduced in a hydrogen flow and 46 nm for the sample synthesized in vacuum. The subsequent heat treatment of reduced samples at 1400°C/4 h in air resulted in oxidation to give again CeO₂ and α -Al₂O₃.

More information about the structure of compounds formed upon heat treatment under both oxi-

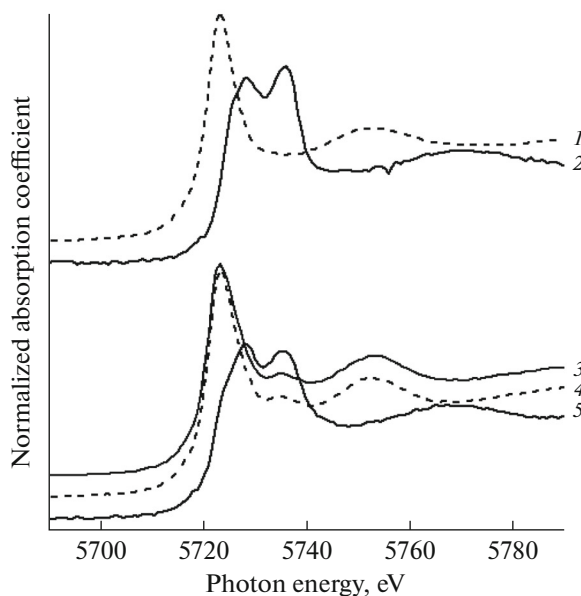
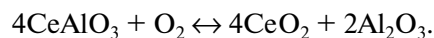


Fig. 5. Ce L_3 -edge XANES spectra of (1, 2) reference samples and (3–5) synthesized samples: (1) Ce(NO₃)₃; (2) Ce(SO₄)₂; (3) CeAl_1100A/1400V; (4) CeAl_1100A/1000H; (5) CeAl_1100A.

dizing and reducing conditions was gained by Raman spectroscopy. The Raman spectrum of the sample synthesized by isothermal annealing of the precursor at 1100°C/3 h showed a clear-cut peak at 463 cm⁻¹ ($FWHM = 14$ cm⁻¹) corresponding to the triply degenerate F_{2g} mode of the cerium dioxide fluorite lattice (Fig. 1, spectrum 2), caused by symmetric vibrations of oxygen atoms around the cerium ion in the CeO₈ cell [23, 24], and a group of weak peaks in the 2000–2250 cm⁻¹ region. As the sample is kept in vacuum, this characteristic CeO₂ line disappeared (Fig. 1, spectrum 3). The subsequent heating to 1400°C and keeping at this temperature for 4 h in air gave rise again to the 462 cm⁻¹ mode in the spectrum ($FWHM = 12$ cm⁻¹) (Fig. 1, spectrum 4).

Thus, integrated analysis of powder X-ray diffraction data and Raman spectra provided the conclusion that the following reaction is reversible:



Data on the local structure of the powders were obtained from cerium L_3 -edge XANES spectrum corresponding to electron transition from the core $2p^{3/2}$ level to the valence $5d$ level (Fig. 5). As can be seen from Fig. 5, the powder obtained by heat treatment in air at 1100°C/3 h showed a typical Ce L_3 -edge XANES spectrum as a split white line corresponding to compounds containing Ce⁴⁺ cations, in particular, CeO₂ [26, 27]. For the reduced samples, the absorption peak

Table 2. Results of determination of the composition of reduced samples by calculations of XANES spectra

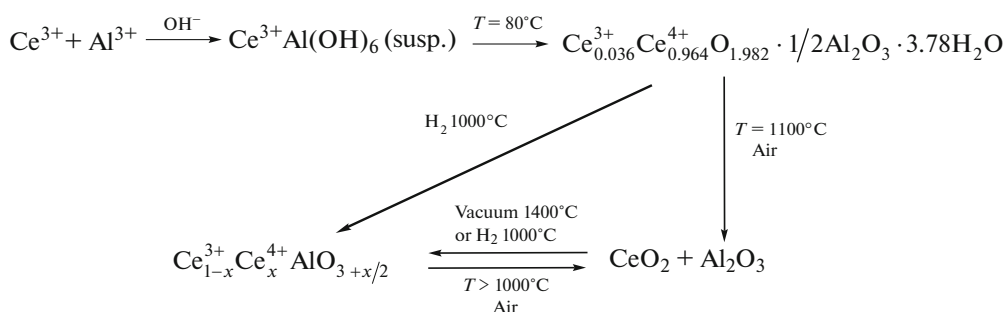
Designation	Composition
CeAl_1100A/1000H	$\text{Ce}_{0.925}^{3+}\text{Ce}_{0.075}^{4+}\text{AlO}_{3.038}$
CeAl_1100A/1400V	$\text{Ce}_{0.883}^{3+}\text{Ce}_{0.117}^{4+}\text{AlO}_{3.059}$

(“white line”) was split because of excitation along two possible channels due to the difference between the electronic structures of Ce^{3+} ($4f^1$) and Ce^{4+} ($4f^0$) cations. This spectral pattern is a distinctive feature of XANES spectra of intermediate-valence compounds [28]. A decrease in the cation oxidation state shifted the absorption edge to lower energy (Fig. 5). It is noteworthy that the XANES spectral patterns for reduced samples of cerium aluminate coincide with the reported CeAlO_3 spectra [7, 29].

The experimental curves were simulated in the 5710–5740 eV region by representing each spectrum as

a superposition of the $\text{Ce}(\text{NO}_3)_3$ and $\text{Ce}(\text{SO}_4)_2$ reference spectra corresponding to the Ce^{3+} and Ce^{4+} states. The proportions of Ce^{3+} and Ce^{4+} in the samples estimated from the obtained weighting coefficients are presented in Table 2. As can be seen from Table 2, the chemical composition of the reduced $\text{Ce}_{1-x}^{3+}\text{Ce}_x^{4+}\text{AlO}_{3+x/2}$ powders calculated from XANES spectra is in qualitative agreement with the TG data (Table 1) but is somewhat higher in magnitude.

Thus, our study demonstrated that hydrogen reduction at 1000°C and annealing in vacuum at 1400°C yields cerium monoaluminate $\text{Ce}_{1-x}^{3+}\text{Ce}_x^{4+}\text{AlO}_{3+x/2}$ powders with $0.052 < x < 0.204$ content of Ce^{4+} cations. The degree of reduction and the thermal oxidation stability of reduced powders depend not only on the reduction conditions but also on the heat pretreatment conditions of the initial powders. Relying on integrated analysis of the results, we propose the following scheme of reactions for the system in question:



ACKNOWLEDGMENTS

This work was supported by the Russian Science Foundation (grant no. 14-22-00098).

REFERENCES

1. A. I. Leonov, *High-Temperature Chemistry of Cerium Oxide Compounds* (Nauka, Leningrad, 1969) [in Russian].
2. B. A. Arsen'ev, L. S. Kovba, and Kh. S. Bagdasarov, *The Chemistry of Rare Elements* (Nauka, Moscow, 1983) [in Russian].
3. Q. Yuan, H.-H. Hao-Hong Duan, L.-L. Li, et al., *J. Coll. Inter. Sci.* **335**, 151 (2009).
4. V. K. Ivanov, A. B. Shcherbakov, A. E. Baranchikov, et al., *Nanocrystalline Ceria: Properties, Synthesis, Application* (Izd. Tomsk. Univ., Tomsk, 2013) [in Russian].
5. V. K. Ivanov, G. P. Kopitsa, A. E. Baranchikov, et al., *Russ. J. Inorg. Chem.* **54**, 1857 (2009).
6. V. K. Ivanov, A. E. Baranchikov, O. S. Polezhaeva, et al., *Russ. J. Inorg. Chem.* **55**, 325 (2010).
7. O. V. Safonova, A. A. Guda, C. Paun, et al., *J. Phys. Chem.* **118**, 1974.
8. E. M. Moroz, *Russ. Chem. Rev.* **80**, 293 (2011).
9. J. Kašpar, M. Graziani, and P. Fornasiero, *Handbook on the Physics and Chemistry of Rare Earths: The Role of Rare Earths in Catalysis*, Ed. by K. A. Gschneidner, Jr. and L. Eyring (Elsevier Science, Amsterdam, 2000), Vol. 29, p. 159.
10. S. A. Venâncio and P. E. V. de Miranda, *Ceram. Int.* **37**, 3139 (2011).
11. A. I. Mikhailichenko, E. B. Mikhlin, and Yu. B. Patrikeev, *Rare-Earth Metals* (Metallurgiya, Moscow, 1987) [in Russian].
12. P. Maestro and D. Huguenin, *J. Alloys Compd.* **225**, 520 (1995).
13. A. Feteira, D. C. Sinclair, and M. T. Lanagan, *J. Appl. Phys.* **101**, 064110 (2007).
14. T. Shishido, S. Okada, Kudou K. Kunio, et al., *Pacific Sci. Rev.* **10**, 45 (2008).
15. L. Vasylechko, A. Senyshyn, D. Trots, et al., *J. Solid State Chem.* **180**, 1277 (2007).
16. G. R. Rao and B. G. Mishra, *Bull. Catal. Soc. Ind.* **2**, 122 (2003).
17. P. A. Deshpande, S. T. Aruna, and G. Madras, *Catal. Sci. Technol.* **1**, 1683 (2011).
18. P. A. Deshpande, S. T. Aruna, and G. Madras, *Clean Soil, Air, Water* **39**, 259 (2011).

19. V. V. Popov, Ya. V. Zubavichus, A. P. Menushenkov, et al., *Russ. J. Inorg. Chem.* **60**, 16 (2015).
20. A. P. Hammersley, S. O. Svensson, M. Hanfland, et al., *High Press. Res.* **14**, 235 (1996).
21. V. Petricek, M. Dusek, and L. Palatinus, *Jana 2006, The Crystallographic Computing System*, Praha, Czech. Republic, Institute of Physics, 2006.
22. K. V. Klementiev, <http://www.cells.es/old/Beam-lines/CLAESS/software/xanda.html>.
23. B. M. Reddy, A. Khan, P. Lakshmanan, et al., *J. Phys. Chem. B* **109**, 3355.
24. G. Gouadec and Ph. Colomban, *Prog. Cryst. Growth Charact. Mater.* **53**, 1 (2007).
25. I. R. Lewis and H. G. V. Edwards, *Handbook of Raman Spectroscopy* (Marcel Dekker, New York, 2001).
26. A. V. Soldatov, T. S. Ivanchenko, S. Della Longa, et al., *Phys. Rev. B* **50**, 5074 (1994).
27. V. Fernandes, I. L. Graff, J. Varalda, et al., *J. Electrochem. Soc.* **159**, 27 (2012).
28. D. I. Khomskii, *Usp. Fiz. Nauk* **129**, 443 (1979).
29. P. E. R. Blanchard, S. Liu, D. J. Kennedy, et al., *J. Phys. Chem.* **117**, 2266.

Translated by Z. Svitanko